Final report for NKFIH project No. NN-125832:
"M-ERA.NET: Ultrafine eutectics by laser additive manufacturing"
(1 September 2017 – 31 August 2021)

I. The major aims of the performed research:

The present NKFIH project forms part of the M-ERA.NET consortial project "ELAM: Ultrafine eutectics by laser additive manufacturing", which is aimed at developing new high strength eutectic alloys by laser-based additive layer manufacturing (ALM) using selective laser melting and laser metal deposition technologies applied for Ti-TiFe and Fe-Fe_2Ti eutectic alloys [1]. It was the "ELAM" project that made the first attempt to produce ultrafine FeTi eutectics by ALM and for automotive (turbocharger propeller) and other applications (such as cutting tool). Accordingly, the activities of the "ELAM" consortium cover the entire manufacturing chain, starting from fundamental materials development, via powder production, optimizing the ALM process and post-processing treatment, to demonstrator testing.

The present NKFIH funded project forms workpackage W2.2 of the M-ERA.NET consortial project "ELAM". It is aimed at supporting fundamental materials development using mathematical models for optimizing the eutectic microstructure via establishing the relation between the technological conditions and microstructure, establishing thus computer aided materials design for alloy produced by lased-based ALM technology. In particular, phase-field modeling was used to model the microstructure of nanoscale eutectic matter as a function of the cooling conditions, which was taken from mesoscale modeling of laser melting. The main goal of the proposal is the development and validation of the computational materials design methodology proposed for laser-based ALM of high melting point alloys.

The main activities performed by the Wigner research team within in WP2.2 of "ELAM" were as follows:

(a) Phase-field modeling of the globular band observed at the lower border of the re-melted layers as indicated by the experiments by the consortial collaborators (Fig. 1).

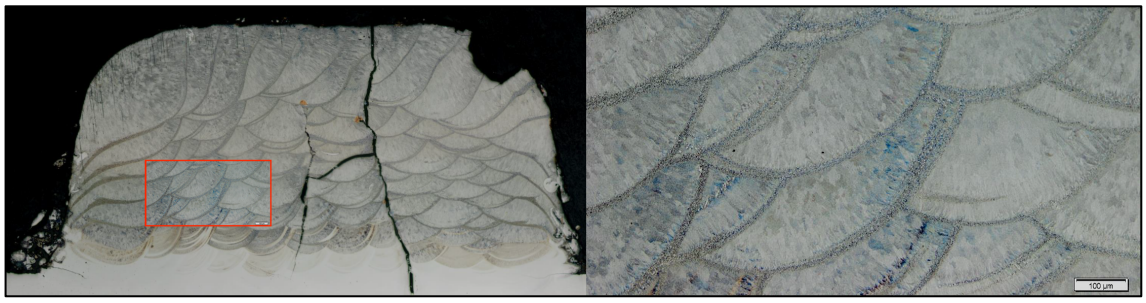

Figure 1: *Experimental image of the cross section of a FeTi sample produced by laser additive manufacturing (By courtesy of G. Rödler, Fraunhofer IL, Aachen, Germany & A. Theofilatos, Access e.V., Aachen, Germany.) Note the the thin globular layers separating the previously melted and the newly melted layers.*

To model these structures, the Wigner team adapted the following two models:

Model 1 is an orientation-field-based phase-field approach [1], with which we were able to demonstrate for a simple model system (of regular solution thermodynamics) that the spatial variation of the eutectic pattern typical to laser additive manufacturing of eutectic alloys can be qualitatively recovered on the basis of such simulations (the relevant results were published in Refs. [2, 3]).

Model 2 is a phase-field model that combines the models of Folch-Plapp [4] and Kim [5] to ensure quantitative simulations.

(b) To accelerate numerical simulations, we developed approximate thermodynamics for the Fe-Fe_2Ti system that reproduces the phase diagram, and we made simulations with this CALPHAD thermodynamics. The eutectic wavelength vs. velocity relationship **Model 2** predicts is in a good agreement with previous experimental results by Tokoro and Kimura [6]. These thermodynamics data serve as the basis for further studies of the FeTi system.

(c) Combining experimental findings by the consortial partners and our simulation results raised the possibility that crystalline particles created during re-melting of the previously formed lamellar eutectic layer might be responsible for the appearance of the interlayer granular domain [3]. To explore this possibility, we have performed analytical investigations and phase-field simulation using **Model 2** to clarify the conditions of such behavior (the results are described in Ref. [7]).

II. The work performed:

II.A Qualitative modeling of solidification microstructure in ALM in Model 1

Here, we adopted an orientation-field-based phase-field method for binary eutectic solidification on the sub-micrometer scale that we developed earlier [1] for describing microstructure evolution during multigrain eutectic solidification. For the detailed description of the model and the values of the model parameters see Ref. [3].

For the sake of simplicity, we performed the simulations for a simple model system, a regular solution approximant of Ag-Cu alloys, under the following conditions: vertical temperature gradient $G = 250\times10^6$ K/m, quenching rate ~ 3.3×10^9 K/s. At $T = 900$ K, we observed a growth rate of 8.6 cm/s and Jackson-Hunt wavelength of $\lambda = 8.8$ nm, yielding $K_0 = 6.7\times10^{-18}$ m^3/s for the Jackson-Hunt constant. The cooling conditions used mimic the behavior reported for ns laser pulses (pulse length 16 ns, energy 8 mJ, laser spot diameter 0.4 mm, calculated melt depth 0.6 μm, $G \approx 10^9$ K/m, quenching rate ~ 3.3×10^9 K/s) [8]. The assumed thermal history is shown in Fig. 2. The temperature increases linearly from the minimum value (shown by the blue line in Fig. 2(a)) prescribed at the left and right hand sides of the simulation window to the maximum value at the center of the simulation box (red line in Fig. 2(a)), providing a temperature gradient from left and right towards the center of the simulation box.

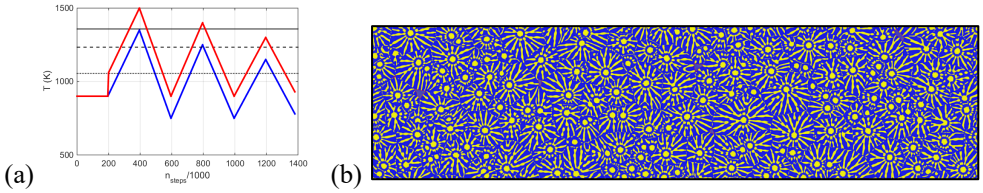

Figure 2: *Thermal history (a) during laser melting and (b) the starting condition (composition field) at $t = 2\times10^5\Delta t$. In panel (a) the horizontal lines going upwards indicate the eutectic temperature, and the melting points of Ag and Cu, respectively.*

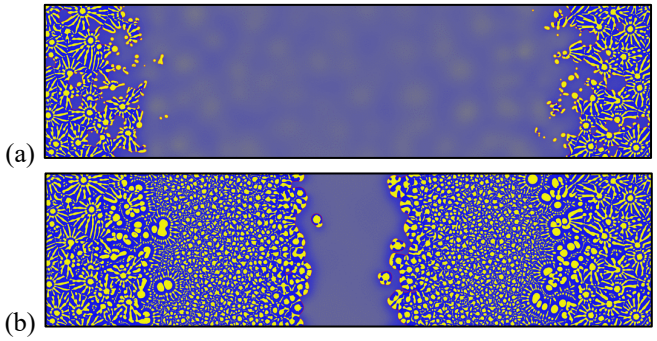

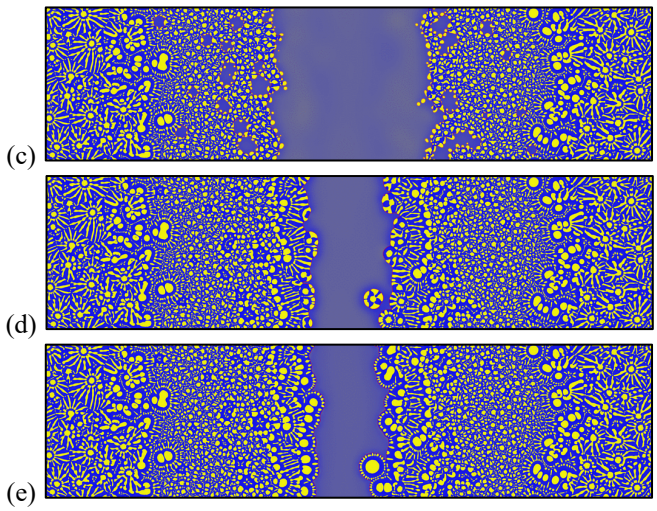

Figure 3: *Snapshots of the time evolution of eutectic microstructure taken at (a) $t = 5\times10^5\Delta t$ after remelting during 1st heating, (b) $7\times10^5\Delta t$ after 1st cooling, (c) $9\times10^5\Delta t$ after 2nd heating, (d) $1.1\times10^6\Delta t$ after 2nd cooling, (e) $1.4\times10^6\Delta t$ after 3rd heating & cooling. Note the periodic formation of large-scale starlike and fine (balls) equiaxed structures [2]. The latter resembles the microstructure observed between the additive layers [3].*

The predicted microstructures are displayed in Fig. 3, and were published in Ref. [2]. Note the formation of alternating layers of large-scale star-like equiaxed structures and fine equiaxed structure composed of small circles of the yellow phase in the matrix of the blue phase. The latter microstructure resembles closely to the granular microstructure observed in the experiments.

Next, we extended Model 1 so that the addition of new layers to the existing ones is incorporated. In the respective study, we used a symmetric eutectic model alloy with phase diagram shown in Fig. 4(a). The assumed cyclic temperature program (corresponding to the heating as the laser beam passes over the simulation domain and the subsequent cooling) is also shown in Fig. 4(b). During the heating period, a new layer of off-eutectic melt is introduced into the simulation box, and part of the lamellar eutectic structure formed in the previous cycle is also re-melted. During the cooling period, first, nucleation of the primary phase near the lamellar front takes place, blocking its epitaxial growth, and serving as growth centers for new lamellar grains which then form the new lamellar layer. By the repetition of this process the layered structure shown in Fig. 5. emerged.

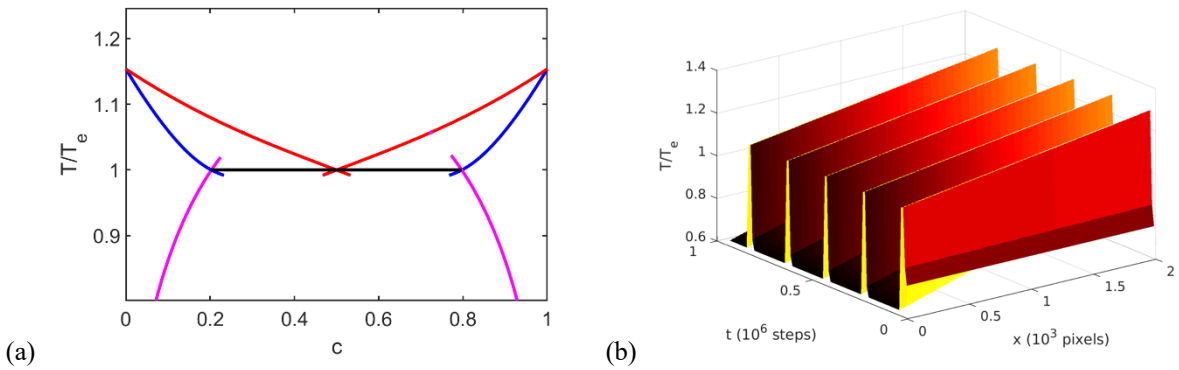

Figure 4: *(a) The phase diagram of the symmetric model alloy and (b) the temperature program that we used in our phase-field simulations [3].*

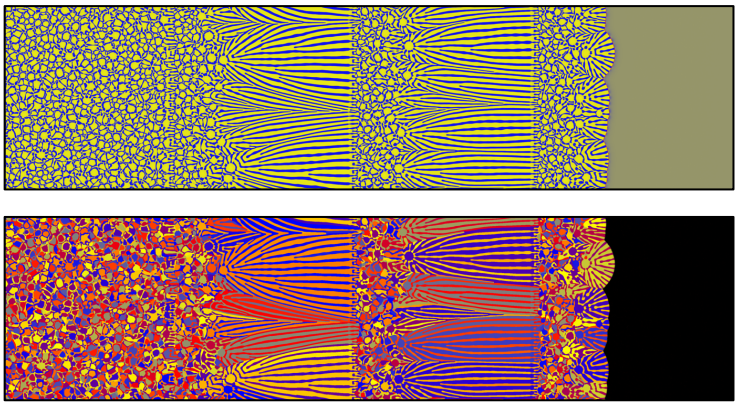

Figure 5: *Two-dimensional phase-field simulations of the layered eutectic structure observed in the experiments. The top and bottom rows show the concentration and orientation maps, respectively. The growth direction is from left to right [3].*

The layer-wise addition of new layers of matter within the phase-field simulations with Model 1 is further illustrated in Fig. 6: As soon as the actual simulation window solidified to a prescribed extent, it was pushed out the simulation window, so far as only a small amount of solid remained, while filling the remaining empty space by hot molten alloy. Owing to the assumed thermal history a thin layer of the remained solid layer re-melted. A montage constructed from snapshots of the composition field is shown in Fig. 6.

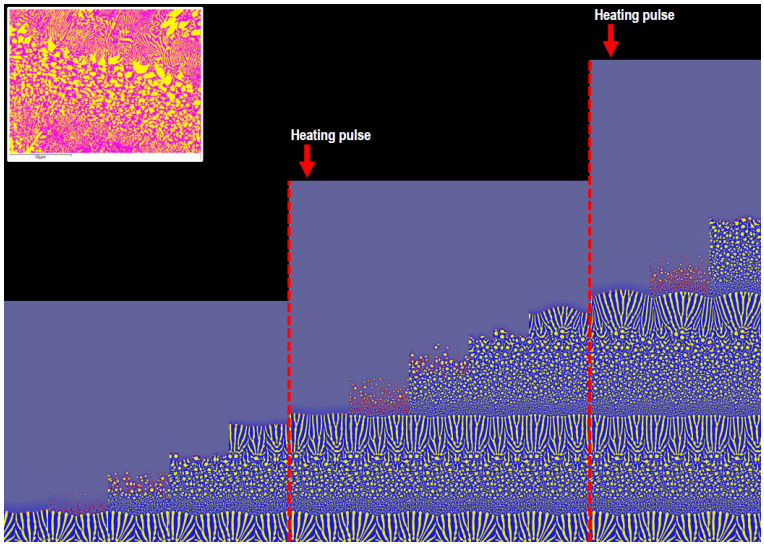

Fig. 6 *Sequence of snapshots of microstructure evolution in the case of layer-wise addition of matter as predicted by a phase-field simulation. The time elapses from left to right. The red dashed line indicates the instances, when hot liquid melt is layered on the top of the partly solidified structure. The composition map is shown: the homogeneous part on the top is the liquid, whereas the solid phases are on the bottom, shown by blue and yellow. The black background is the air. The insert shows the experimental layered structure.*

Note the similarity between the predicted alternating layers of large-scale star-like equiaxed structures (formed during moderate undercoolings) and the fine equiaxed structure composed of small circles of the yellow phase (formed by copious nucleation at high undercoolings) in the matrix of the blue phase and the experimental microstructure displayed in the insert of Fig. 6.

Using Model 1, we investigated the effects of nucleation mechanism and the processing conditions on eutectic pattern formation. We compared two cases of nucleation: (1) noise induced homogeneous nucleation (result shown in previous report), and (2) particle induced heterogeneous nucleation. To see whether heterogeneous nucleation via free

growth leads to microstructures that qualitatively agree with experimental observations, we performed a simulation with 400 randomly distributed dormant nucleation sites in the simulation domain. These sites can be considered as impurity particles, as in the case of the athermal nucleation model by Quested and Greer [9], or partially re-melted and spheroidized fragments of the eutectic lamellae from the primary phase produced in the previous heating cycle. The simulated structure at the interlayer boundary is very close to those obtained with homogeneous nucleation (see previous report) and in qualitative agreement with the experimental observations.

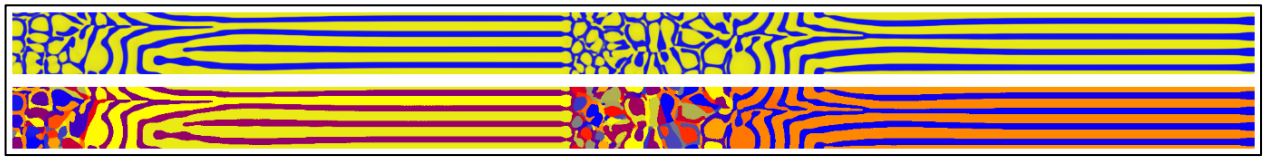

Figure 7: *Eutectic microstructure predicted assuming particle induced heterogeneous nucleation and free growth with average concentration $c_0 = 0.6$ (hyper-eutectic case). Top: composition field, bottom: orientation field.*

Next, we investigated the effect of tuning the parameters that influence nucleation, such as the local temperature, the composition, and the amplitude of the fluctuations. Of them, composition and the temperature can be changed in a controlled way in the experiments. Our simulations show that with decreasing temperature of the already solid domain the thickness of the globular domain increases (Fig. 8). Finally, we found that with increasing driving force (deviation from the eutectic composition) and with higher noise amplitude, the nucleation rate increases, together with the thickness of the globular layer, whereas the average size of the globular particles decreases.

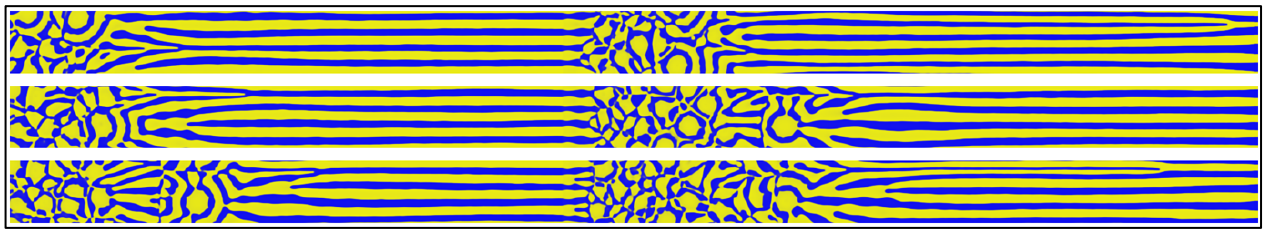

Figure 8: *The effect of temperature on the eutectic microstructure as predicted by phase-field simulations. The temperature of the solidified layer downwards: panels display simulations, in which the temperature during the cooling stages were 10 K and 20 K lower than in the upmost simulation. Here $c_0 = 0.6$.*

Finally, we note that the eutectic model developed in this activity of the project turned out an extremely useful tool in studying biological crystallization processes, namely the formation of mollusk shells including bivalves, cephalopods, and gastropods [4], a fact acknowledged in the respective paper.

II.B Approximate thermodynamics for the Fe-Ti system

In the next phase of our research, we collected the thermodynamic data for the relevant phases in the Fe-Fe_2Ti eutectic system from both the literature and the public CALPHAD databases. On the basis of these data, we reconstructed the Gibbs free energy functions of the constituent phases and incorporated them into our multi-phase-field code. Unfortunately, the Gibbs free energy of the Fe_2Ti Laves phase cannot be given as a simple analytic function, as it involves the optimization of the sub-lattice occupancies. Though this can be done via an iterative method in the numerical simulations, it increases the computational time significantly. For an improved numerical efficiency, it would be beneficial if we could use a simpler, approximate thermodynamics in our future simulations. To realize this, we investigated how far one can get using the parabolic free energy approach described by Folch and Plapp [4]. Along these lines, first we fitted the parameters of approximate thermodynamics so that the solidus and liquidus lines are reproduced in the vicinity of the eutectic temperature. After performing simulations for 2D lamellar eutectic solidification with the accurate and approximate thermodynamics, we concluded that the latter provides results that are almost identical to those obtained with full thermodynamics (see Figs. 9 and 10), however, in a much shorter time (the

computation time was reduced by a factor of ~ 40). Therefore, in the rest of the project the fast, simplified thermodynamics was used, while making further validation simulations in a few selected cases using the full but slow Gibbs free energy functions. Note the good agreement between experiment and theory (Fig. 10(b)).

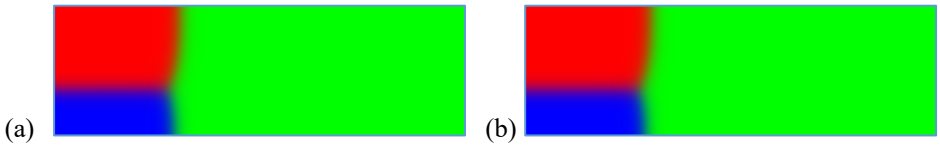

Figure 9: *Comparison of multi-phase field simulation of lamellar eutectic solidification in the Fe-Fe₂Ti system at the eutectic composition. (a) With CALPHAD thermodynamics; (b) with the parabolic approximation.*

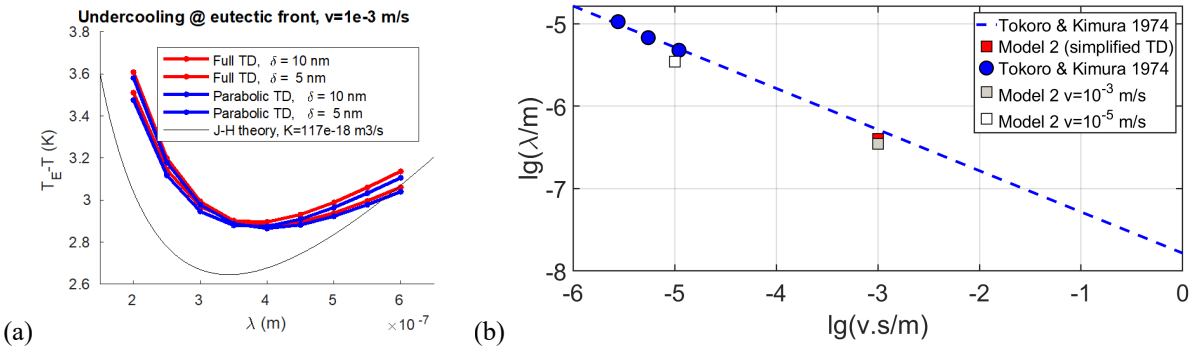

Figure 10: *Testing the approximate thermodynamics for Fe-Fe₂Ti eutectics: (a) Comparison of the Jackson-Hunt plot with the CALPHAD (red lines) and approximate thermodynamics (blue lines); (b) Parameter free comparison of the wavelength vs. velocity relationship from experiments (blue dashed line) to quantitative phase-field simulations performed with Model 2 using full CALPHAD thermodynamics (empty and grey squares) and simplified thermodynamics (red square).*

II.C Quantitative phase-field modeling of eutectic melting using Model 2

Under the additive manufacturing conditions, the microstructure of the eutectic Fe-Fe₂Ti samples shows a layered structure. In the thin interlayer boundaries (ILBs) a globular morphology can be observed, from which a thicker layer of ultrafine lamellar structure develops. We have successfully modelled this structure. Understanding how the globular grains are formed in the ILBs is of key importance for controlling this special microstructure. In our previous simulations we explored different nucleation mechanism that may produce the seeds of the globular particles, but it is more likely that they are fragments of lamellae that could re-melt only partially during the preceding melting by the laser beam. Therefore, we performed theoretical/numerical studies of eutectic melting, a phenomenon, which has not been investigated extensively in the literature.

C.1 Analytic studies: Based on similar ideas that were used in the formation of the first analytic theories of eutectic solidification [12], we aimed at determining the lamellar solid-liquid interface profile during melting. We started from the exact solution of the diffusion equation in a reference frame traveling with the interface as it melts. Using mass conservation as the boundary condition at the interface and assuming local equilibrium along the interface and at the tri-junction, we could obtain the interface curvature as function of the position x, from which the profile shape could be reconstructed by solving the appropriate ordinary differential equations. Figure 14 shows the profiles obtained for the solidification and melting of a lamellar structure of a symmetric model system.

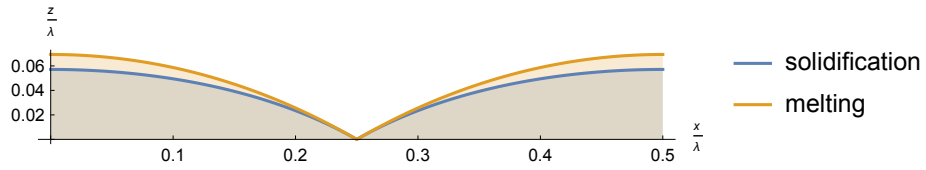

Figure 11: *The solid-liquid interface profile for lamellar eutectic solidification and melting for a simple symmetric model system. The profiles were obtained by solving the diffusion equation in the melt and the respective local equilibrium equations and boundary conditions at the interface.*

C.2 Numerical studies using Model 2: The equations defining the quantitative phase-field model termed here Model 2 can be seen in Ref. [4], while the results we obtained are shown in detail in Ref. [7]. Using this model, we have successfully simulated the melting of a lamellar structure both in the coupled and non-coupled regime [11]. In the coupled regime, the solid-liquid interface profiles are similar both in the solidification and melting setup, the solidification profiles being flatter and showing lower curvatures in the centers of the lamellae, as expected from simple considerations (Fig. 11). However, in the non-coupled regime, the melting profiles can become markedly different: the two phases will melt at different positions in the temperature gradient (Fig. 12), the one deeper in the melt termed as the leading phase [11]. Under suitable conditions the leading phase is reported to undergo spherodization, during which increasing instabilities break up the long penetrating lamellae, resulting in the steady state production of small solid parts that melt in the increasing temperature field. This spherodization phenomenon has also been successfully reproduced in our phase-field model (Fig. 13).

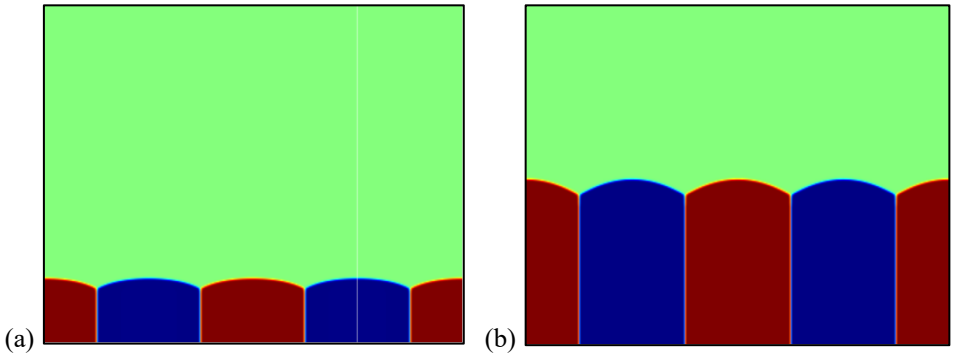

Figure 12: *Phase-field simulation of (a) lamellar eutectic solidification and (b) the coupled melting of a lamellar structure in a symmetric model system [7]. All parameters were the same in the two simulations, expect for the velocity of the temperature gradient, which has been inverted in the case of melting. The solidification profiles are "flatter" and located at lower temperatures than the melting profiles.*

Figure 13: *Phase-field simulation of the non-coupled melting of a lamellar structure of different widths [7]. The initial ratio of the red and blue phases is 0.55:0.45, and only one half of a lamella is shown. The temperature increases from left to right while reference frame travels from right to left, providing stationary profiles within the simulation domain that corresponds to steady state melting. The red phase becomes the "leading phase" extending deep into the melt.*

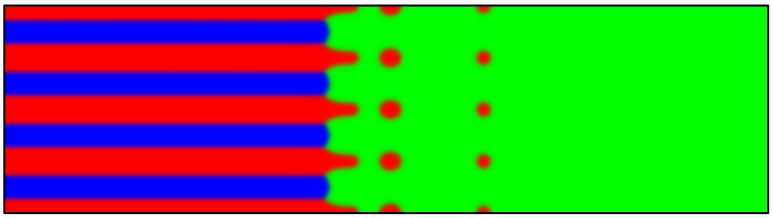

Figure 14: *In the non-coupled case of lamellar melting, the instabilities along the long penetrating leading phase may result in the breakup of the lamellae [7], resulting in disconnected solid particles, a phenomenon termed as spherodization [11].*

We have extended our study to the melting of 3D rod structures, and observed, that our main finding is valid also in this case: if the main composition of the solid is off-eutectic, than the structure melts in a non-coupled way. The phase which is present in a lower amount than required for the eutectic composition, melts at the eutectic temperature, while the phase present in a higher amount melts at its liquidus temperature corresponding to the mean (off-eutectic) composition (see Fig. 14).

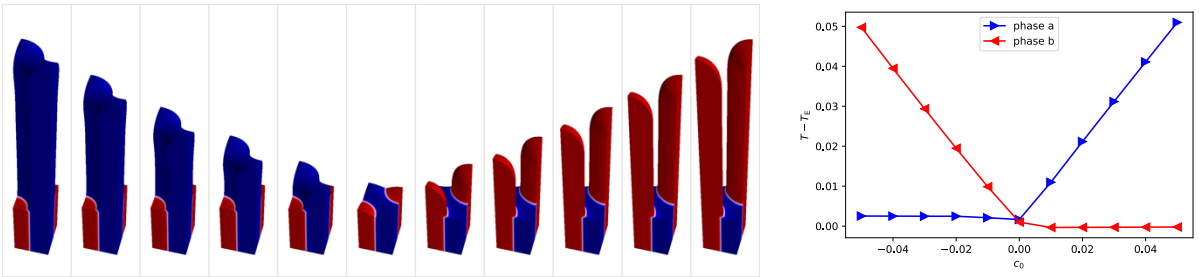

Figure 15: *Steady-state melting forms of 3D rod structures as function of the initial volume fraction (or equivalently, the c_0 mean composition) of the solid to melt. Left: result of simulations in the minimal domain that corresponds to the hexagonal arrangement of the rods, c_0 = -0.05, -0.04, … 0.05. The full structure can be reconstructed by the required translation and mirroring of these minimal units. Right: the corresponding undercooling vs. c_0 plot.*

References:

[1] D. Lewis, T. Pusztai, L. Gránásy, J. Warren, W. Boettinger: *Phase field models for eutectic solidification.* JOM - J. Min. Met. Mat. S. **56**, 34-39 (2004).

[2] L. Gránásy, G.I. Tóth, J.A. Warren, F. Podmaniczky, G. Tegze, L. Rátkai, T. Pusztai: *Phase-field modeling of crystal nucleation in undercooled liquids – A review.* Prog. Mater. Sci. **106**, art. no. 100569 (2019).

[3] G. Requena, K. Bugelnig, F. Sket, S. Milenkovic, G. Rödler, A. Weisheit, J. Gussone, J. Hau-brich, J.C. da Silva, T. Pusztai, L. Gránásy, A. Theofilatos, U. Hecht: *Ultrafine Fe-Fe2Ti eutectics by directed energy deposition: insights into microstructure formation based on experimental techniques and phase field modelling.* Additive Manufacturing **33**, art. no. 101133 (2020).

[4] R. Folch, R, M. Plapp: *Quantitative phase-field modeling of two-phase growth.* Physical Review E **72**, 011602 (2005).

[5] S. G. Kim: *A phase-field model with antitrapping current for multicomponent alloys with arbitrary thermo-dynamic properties.* Acta Mater. **55**, 4391-4399 (2007).

[6] K. Tokoro, Y. Kimura: *Structural and magnetic properties of unidirectionally solidified Fe-Fe2Ti eutectic alloys*. Tetsu-to-Hagane, J. Iron & Steel Inst. Jpn. **60**, 386-396 (1974).

[7] T. Pusztai, L. Rátkai, L. Horváth, L. Gránásy, *Phase-field modelling of melting lamellar and rod eutectic structures.* Submitted to Acta Mater. (2021). See also arXive ……

[8] Cs. Fetzer, L. Gránásy, T. Kemény, E. Kótai, M. Tegze, I. Vincze, W. Howing, F. van der Woude: *Laser melted amorphous and crystalline Fe-B alloys.* Phys. Rev. B **42**, 548-554 (1990).
[9] T. E. Quested and A. L. Greer: *Athermal heterogeneous nucleation of solidification*, Acta Mater. **53**, 2683-2692 (2005).
[10] L. Gránásy, L. Rátkai, G. I. Tóth, P. U. P. A. Gilbert, I. Zlotnikov, T. Pusztai: *Phase-field modeling of biomineralization in mollusks and corals: Microstructure vs. formation mechanism.* J. Am. Chem. Soc. Au **1**, 1014-1033 (2021).
[11] C. A. Norlund, R. Trivedi: *Eutectic interface configurations during melting.* Metall. Mater. Trans. A **31**, 1261–1269 (2000).
[12] K. A. Jackson, J. D. Hunt: *Lamellar and Rod Eutectic Growth.* Trans. Metall. Soc. AIME **236**, 1129–1142 (1966).

III. Dissemination

A. Papers appeared/submitted with acknowledgment to the NN-125832 project:

1. L. Gránásy, G.I. Tóth, J.A. Warren, F. Podmaniczky, G. Tegze, L. Rátkai, T. Pusztai: *Phase-field modeling of crystal nucleation in undercooled liquids – A review.* Prog. Mater. Sci. **106**, art. no. 100569 (2019). (impact factor: 31.560)

2. G. Requena, K. Bugelnig, F. Sket, S. Milenkovic, G. Rödler, A. Weisheit, J. Gussone, J. Hau-brich, J.C. da Silva, T. Pusztai, L. Gránásy, A. Theofilatos, U. Hecht: *Ultrafine Fe-Fe2Ti eutectics by directed energy deposition: insights into microstructure formation based on experimental techniques and phase field modelling.* Additive Manufacturing **33**, art. no. 101133 (2020).
(impact factor: 10.998)

3. T. Pusztai, L. Rátkai, L. Horváth, L. Gránásy, *Phase-field modelling of melting lamellar and rod eutectic structures.* Submitted to Acta Mater. (2021).
(impact factor: 8.203)

4. L. Gránásy, L. Rátkai, G. I. Tóth, P. U. P. A. Gilbert, I. Zlotnikov, T. Pusztai: *Phase-field modeling of biomineralization in mollusks and corals: Microstructure vs. formation mechanism.* J. Am. Chem. Soc. Au **1**, 1014-1033 (2021).
(no impact factor yet)

B. Presentations at conferences:

1. T. Pusztai, L. Gránásy: *Phase-field modelling of the ultrafine eutectic microstructure formed during laser additive manufacturing.* 6th Directionally Solidified Eutectics Conference (DSEC-VI), 10 - 13 September 2019, University of Salerno, Fisciano, Italy.

2. U. Hecht, A. Theofilatos, D. Röhrens, G. Requena, J. Gussone, J. Haubrich, F. Sket, S. Milenkovic, G. Rödler, A. Weisheit, L. Rátkai, L. Gránásy: *Ultrafine Fe-Fe2Ti eutectics by laser additive manufacturing.* 6th Directionally Solidified Eutectics Conference (DSEC-VI), 10 - 13 September 2019, University of Salerno, Fisciano, Italy (invited talk).

3. T. Pusztai, L. Gránásy: *Phase-field modelling of the formation of the layered eutectic microstructure during laser additive manufacturing.* EUROMAT 2021 (virtual conference), 13 - 17 September 2021.